MICROSTRUCTURE AND FRACTURE BEHAVIOUR OF Cr-Mo-V POWER GENERATION STEEL

S.T. MANDZIEJ[1], A. VÝROSTKOVÁ[2] AND J.S. ROBINSON[3]

[1]Advanced Materials Analysis, Enschede, Netherlands. [2]Slovak Academy of Sciences, Kosice, Slovakia. [3]Department of Materials Science and Technology, University of Limerick, Plassey Park, Republic of Ireland

KEYWORDS

embrittlement, intercrystalline fracture, carbides, electron microscopy

ABSTRACT

Low-alloy creep resisting steels used in power generation can embrittle after standard heat treatments and long-term exposure to elevated temperatures. This embrittlement is manifest as an intercrystalline low energy fracture mode when impact testing at low and ambient temperatures. The brittle fractures propagate through prior austenite grain boundaries. Concentration of impurities such as phosphorus, in addition to precipitation of carbides occurs at these grain boundaries. Samples of the Cr-Mo-V steels studied in this work were subject to long-time exposure at power plant application temperature for durations of up to 5000 hours.

Phosphorus concentrations on intercrystalline fracture facets were measured by Auger electron spectroscopy on samples fractured in-situ. The carbide precipitates on intercrystalline facets were analysed by TEM and EDS methods on carbon extraction replicas. These carbides were identified by selected-area electron diffraction. Preliminary results of these identification procedures did not always coincide with thermodynamic calculations. The carbides on the intercrystalline facets were also examined by FEG-SEM with EDS microanalysis, which revealed the formation of carbide agglomerations at the longest times and highest temperatures of exposure. However, both with and without theses agglomerations, the brittle fracture appearance was very similar. An influence of the carbide precipitates on the hot ductility of steels was examined in strain-induced crack opening tests. Finally, the substructure of the embrittled samples was studied by transmission electron microscopy on thin foil specimens.

This work has been undertaken by three partners in the COST 517 action to provide an overall description of the microstructure of the embrittled steels, in particular of the precipitates and contaminants at the brittle intercrystalline facets.

INTRODUCTION

In an extensive research programme carried out at the Institute of Materials Research of the Slovak Academy of Sciences, numerous grades of Cr-Mo-V type low alloy creep resisting steels have been studied to determine their susceptibility to embrittlement in relation to the phosphorus concentration at prior austenite grain boundaries. The programme included long-

term annealing at temperatures representative of power generation applications. Characterisation of the steels involved Auger electron microanalysis of fracture surfaces as well as precipitate phases identification on carbon extraction replicas by transmission electron microscopy and selected-area diffraction plus energy dispersive X-ray spectroscopy microanalysis (EDS). This investigation has led to verification of the thermodynamic calculation procedures used to quantify phosphorus segregation [1]. Some steels included in this programme displayed differences between the theoretical / calculated sequence of carbide transformations, based on the works of Baker and Nutting [2] and later [3], as compared with the preliminary experimental results.

MATERIALS & TESTING

Among the materials showing the discrepancy between the theoretical / calculated carbide phases after the long-term exposures was the one coded #55 in the IMR-SAS programme. This steel had the following chemical composition:

0.133%C, 2.49%Cr, 0.406%Mo, 0.247%V, 0.042%P, 0.33%Mn, 0.23%Si and 0.004%S.

Samples of this material were air-quenched from 1050°C after 30min of austenitisation and then tempered for 2 hours at 650°C. After this heat treatment the average austenite grain size was 130μm. This ensured that impact testing at ambient temperatures resulted in a mainly intercrystalline mode of fracture, Figure 1, with prevailing “smooth” fracture facets.

The long-term embrittling annealing was carried out for 1000 and 5000 hours at 500°C or 580°C. After annealing, the phases: M_7C_3+M_6C+ MC + ferrite, were predicted, but the extraction replicas only contained evidence of M_7C_3+M_3C+MC or M_7C_3+ MC for 500°C and 580°C respectively.

To determine the reason of this discrepancy, further testing was agreed between the partners of the COST 517 Action. It comprised an examination of the intercrystalline fracture surfaces by means of field-emission gun scanning electron microscope with EDS microanalysis, analytical transmission electron microscopy on thin foil specimens, and further examination in the TEM of carbon extraction replicas taken from the intercrystalline fracture surfaces.

Auger electron microanalysis results from the intercrystalline fracture surfaces of samples were already available. These samples, which were fractured in-situ in an Auger microprobe, showed very similar phosphorus concentrations after annealing at 500°C/1000h, 500°C/5000h and 580°C/1000h. A noticeable decrease of the P concentration at grain boundaries was observed in the sample 580°C/5000h, Figure 2.

To establish if the long-term annealing had already caused a loss of ductility, strain-induced crack opening tests (Figure 3 and Figure 4) were run on a Gleeble thermal-mechanical simulator. From flow-stress and stress-relaxation curves of the SICO test the recrystallisation temperature of this steel was determined to be approx. 560°C, for a strain rate of $1s^{-1}$ and a strain of 0.5 The SICO tests were then run with strain rates of $1s^{-1}$ and $5s^{-1}$, at 540°C and 580°C to total strains of: 0.75, 1.00 and 1.25. None of the tested samples showed any cracks on the perimeter of the bulge portion. Modified SICO samples, with conical end portions, Figure 3b, were used to prepare TEM samples of this steel warm-deformed to various small strains below and above the recrystallisation temperature.

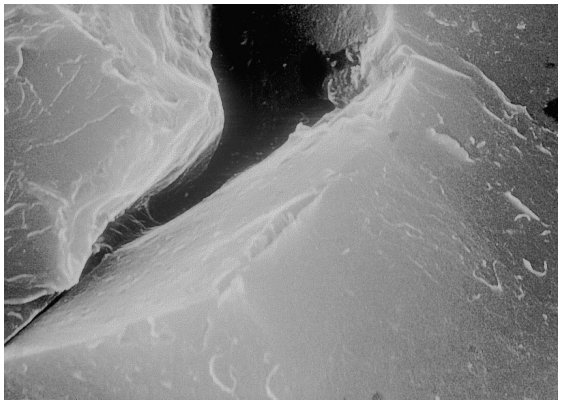

Figure 1 “Smooth” intercrystalline fracture surface of sample 580°C /5000h, cracked in–situ in Auger microprobe; 1500x.

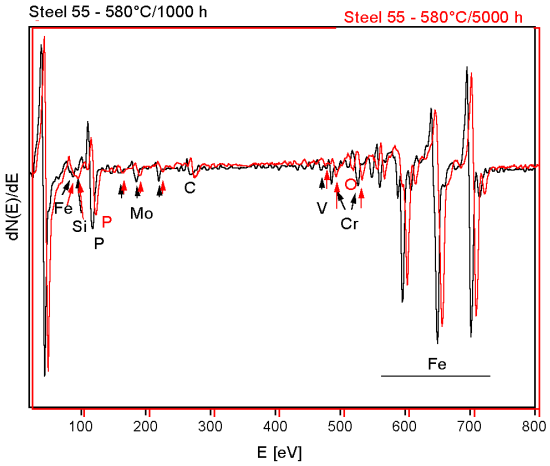

Figure 2 Auger electron spectra of samples 580°C /1000h (black) and 580°C /5000h (red); visible smaller P peak in the last.

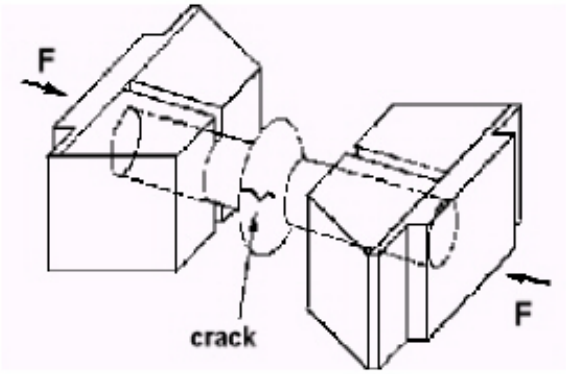

Figure 3 Schematic of SICO test: an axial compression of heated central portion of rod-like sample mounted in cold jaw-blocks.

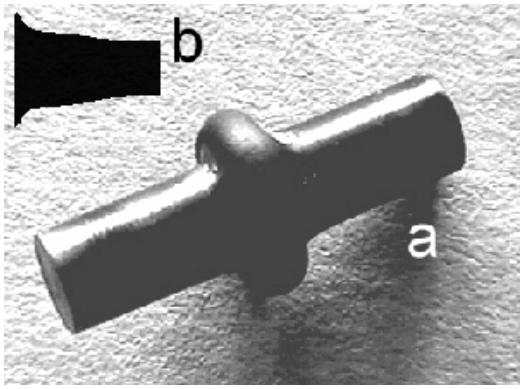

Figure 4 Standard SICO sample (a) deformed to strain of 1.25, and a shadow image (b) of mounting portion of the modified sample.

RESULTS & DISCUSSION

FEG-SEM fractography, microanalysis and SEM metallography

The samples fractured at liquid N_2 temperature and analysed in the Auger microprobe, were then subject to fractographic examination in FEG-SEM. The fractures were mainly brittle and intercrystalline, with a few transgranular cleavage cracks. Frequently evidence of local ductility was found, like that displayed in Figure 5 for sample 500°C/5000h. When observed in the FEG-SEM, the “smooth” intercrystalline surfaces of the prior austenite grain boundaries appeared not to be smooth at all. They showed substantial ductile tearing along many borders of post-martensitic subgrains, especially in the samples which were annealed at lower temperatures, i.e. 500°C, Figure 6. On these intercrystalline fracture surfaces numerous fine precipitates were observed giving different contrast in backscattered electron mode, thus indicating concentrations of lighter or heavier elements, Figure 7. In addition, the ductile tearing was observed along the “river lines” on transgranular cleavage facets, Figure 8.

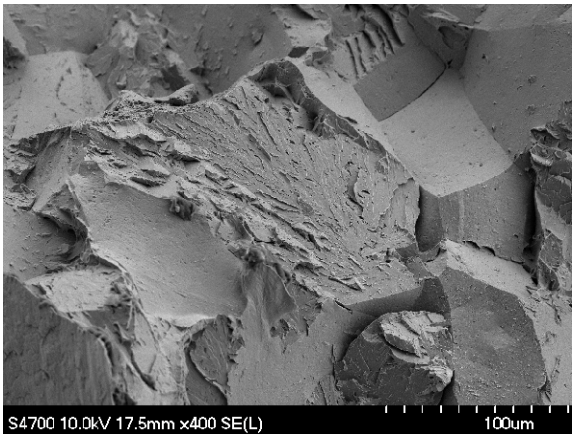

Figure 5 Mixed intercrystalline / transcrystalline fracture of sample 500°C/5000h, cracked in–situ in Auger microprobe.

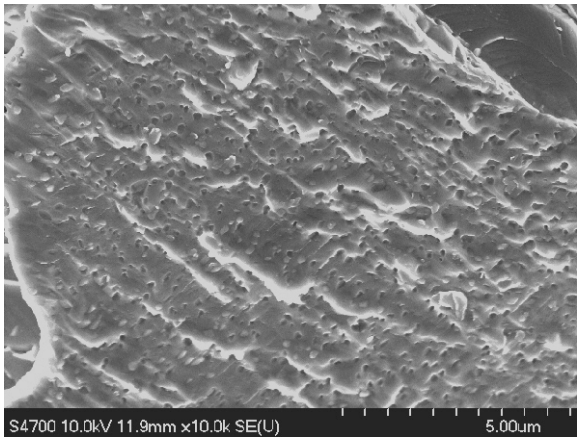

Figure 6 Ductile tearing along post-martensitic interlath boundaries on intercrystalline fracture surface in sample 500°C/5000h.

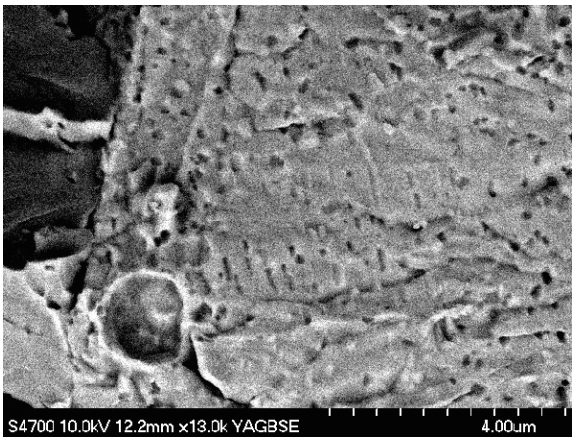

Figure 7 Morphology of carbides on intercrystalline fracture surface as seen in backscattered electron mode on sample 500°C/5000h

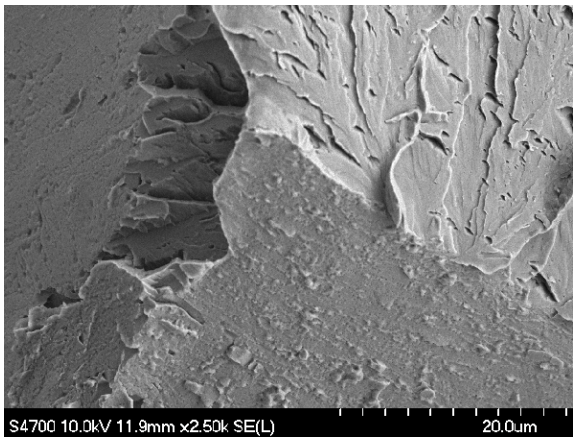

Figure 8 A nucleation site of transcrystalline cleavage fracture, showing ductile tearing type of “river lines” on the cleavage.

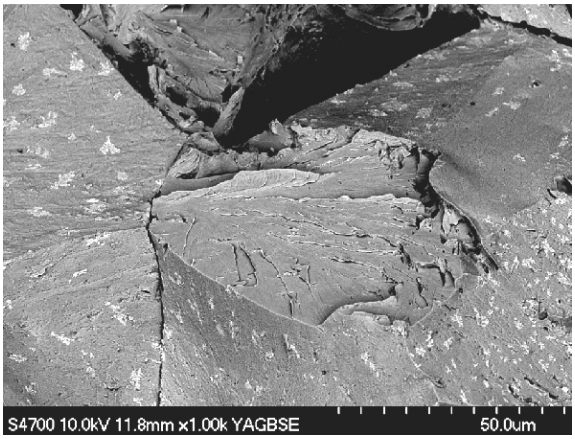

Figure 9 Backscattered electron image of inter- and trans-crystalline fracture surface of sample 580°C /5000h.

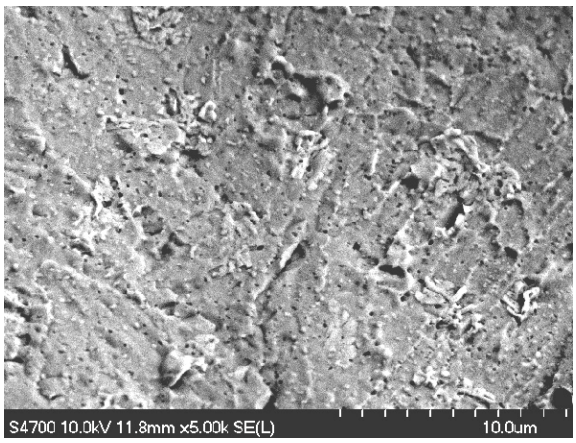

Figure 10 Rough intercrystalline fracture surface visible in secondary electron mode on sample 580°C /5000h.

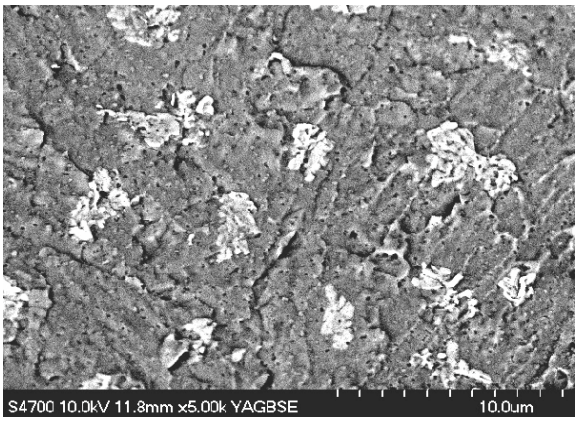

Figure 11 Large agglomerates of particles visible on intercrystalline fracture surface of sample 580°C /5000h, in backscattered electron mode.

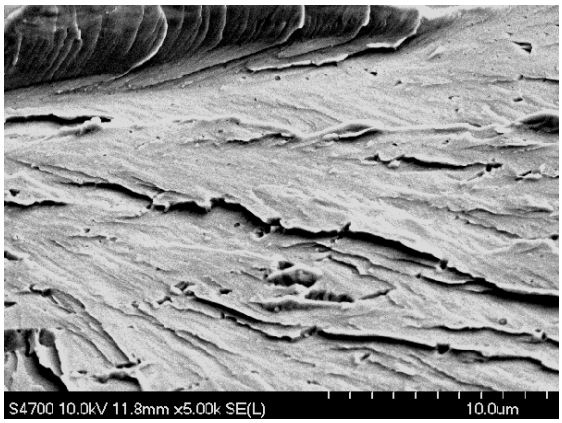

Figure 12 Transcrystalline cleavage facet with protruding plate like particles cut by the crack.

For the samples annealed at higher temperature, i.e. 580°C, the intercrystalline fracture mode also dominated, Figure 9, however here the fracture surfaces appeared to be even more irregular, Figure 10.

Using the backscattered electron imaging, numerous large agglomerates of plate-like precipitates were revealed on these irregular surfaces, Figure 11. These plate-like precipitates also appeared to be visible on transgranular cleavage facets, at sites which could not be ascribed as the prior austenite grain boundaries, Figure 12.
To identify the precipitates in the agglomerates, EDS microanalysis was carried out in the FEG-SEM at various accelerating voltages. It revealed a large concentration of Mo as well as

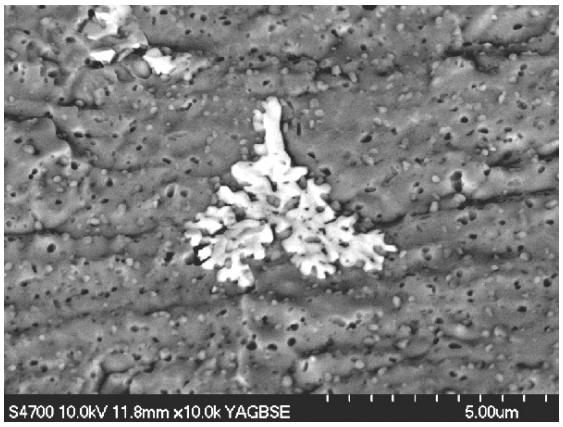

Figure 13 Analysed agglomerate and matrix.

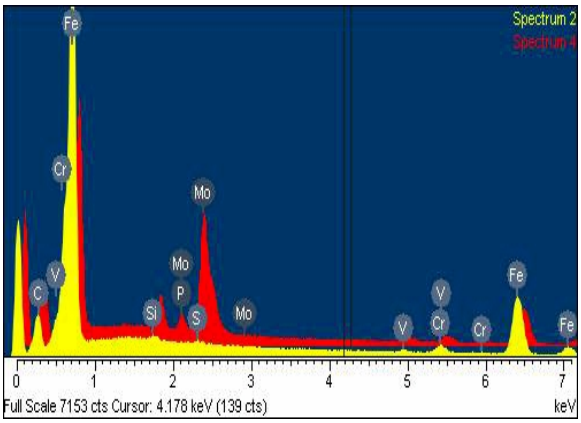

Figure 14 Result of analysis from Figure 13

the presence of Si and P. An example is given in Figure 13 and Figure 14, showing an agglomerate as well as spectra, taken at 7kV, of a large plate-like precipitate (red) and of a nearby matrix with three fine precipitates (yellow). More detailed microanalysis, carried out at 5kV and 3kV, revealed that at least two types of carbides are present in the agglomerates, i.e. the majority containing from 11 to 14 at% C, up to 40 at% Mo, plus Si and P, and the minority containing about 20 at % C, some Si, no Mo and no P. Representative spectra are given in Figure 14.

Further examination was carried out in the SEM. All microstructures were tempered martensite, with relatively smaller carbides precipitated along former boundaries of martensite laths and larger carbides tracing the prior austenite grain boundaries, Figure 16. The agglomerates of the plate-like carbides did not appear in the samples annealed at 500°C, they did appear in samples annealed at 580°C/1000h and 580°C/5000h. The particles were 3 to 6μm long by 0.2 to 0.5μm thick after annealing for 1000h, and 5-10μm long by 0.4 to 1.0μm thick after 5000h, Figure 17. EDX spectra taken from these agglomerates, Figure 18 and

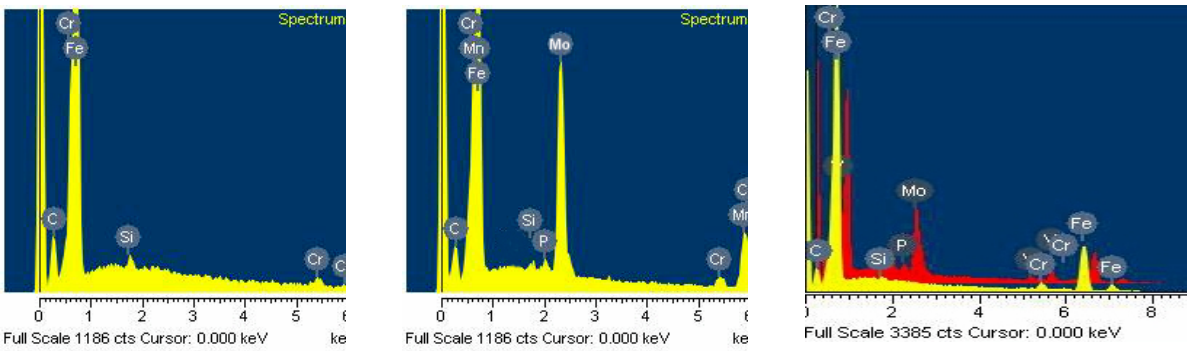

Figure 15 EDS microanalysis results from various sites on intercrystalline fracture surfaces of sample 580°C/5000h,

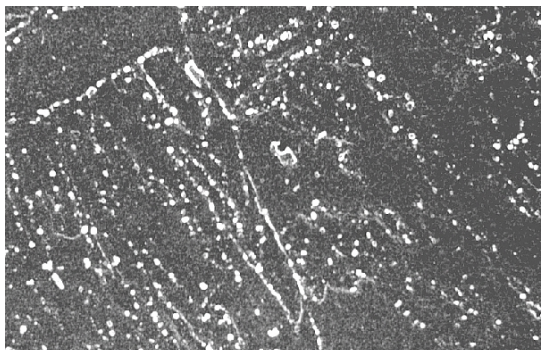

Figure 16 Tempered martensite microstructure of sample 580°C/5000h, with PAGBs traced by large amount of carbides, 3000x.

Figure 17 Elongated agglomerate of particles at PAGB in sample 580°C/5000h, 3000x.

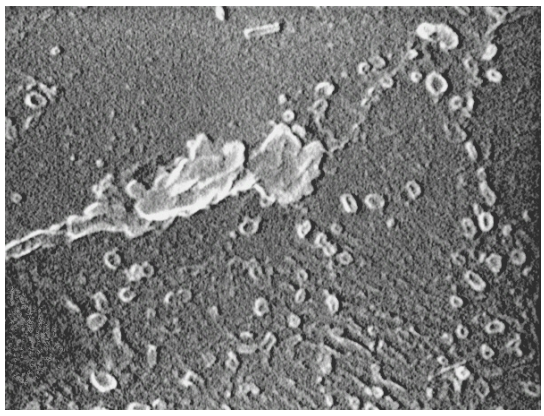

Figure 18 An agglomerate of plate like particles at the PAGB in sample 580°C/5000h 10000x.

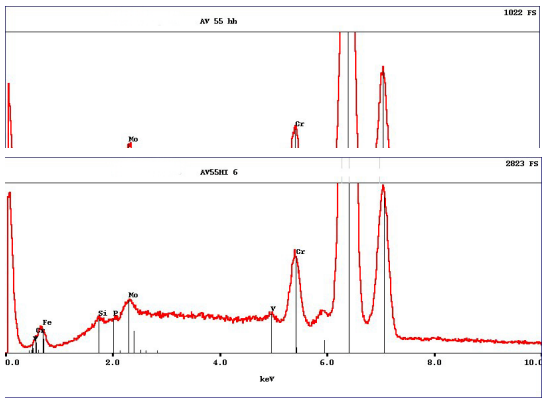

Figure 19 EDS microanalysis from the PAGB agglomerates in sample 580°C/1000h (upper) and 580°C/5000h (lower).

Figure 19, indicated that they were rich in Mo, with decreasing amounts of Fe, Cr, Si, and P in that order.

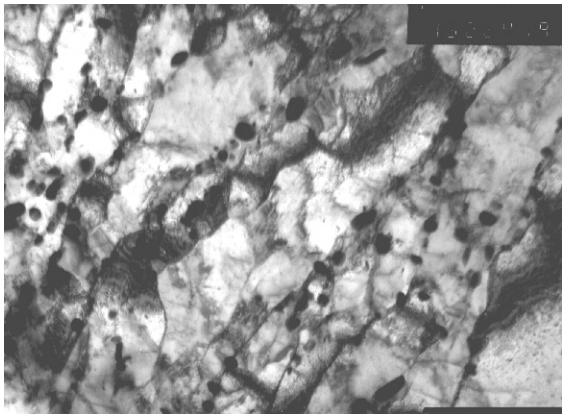

Figure 20 Subgrains of tempered martensite with spheroidized carbides in sample 580°C /1000h

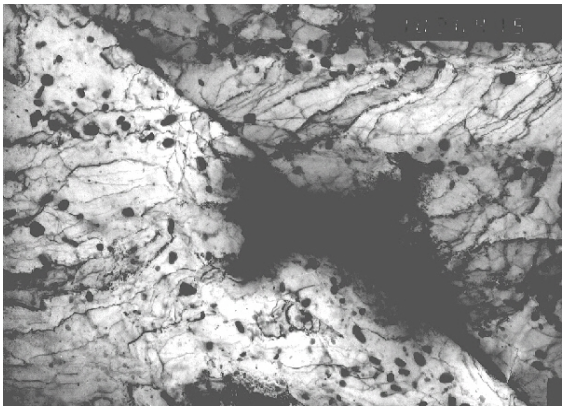

Figure 21 Large agglomerate of particles at PAGB in sample 580°C /5000h

TEM phase identification

The carbides extracted on carbon replicas were identified by selected area diffraction in TEM and EDS microanalysis. Thin foils were prepared by electro-polishing. Some discrepancy appeared in the microanalysis results, when comparing the thin foils with replicas for the same material condition. For example, in sample 580°C/5000h, the carbide agglomerates visible in thin foils has composition: 40%Mo,10%Si and 5.7%P, while on the replicas they were: 50%Mo, 7.5%Si and 3.5%S. This discrepancy can be ascribed to the accuracy of the specimen thickness measurement and quantification correction programme. As regards the comparison between 580°C/1000h and 580°C/5000h states, more Mo and less S and P were found in the agglomerates after 5000h of annealing.

The substructure of the steel in all examined states comprised well-developed subgrains with partly spheroidised carbides deposited mainly along the subgrain boundaries, Figure 20. In samples annealed at 500°C these carbides were mainly of M_7C_3 type, with a lesser amount of cementite. After annealing at 580°C, substantial amounts of $M_{23}C_6$ were detected adjacent to

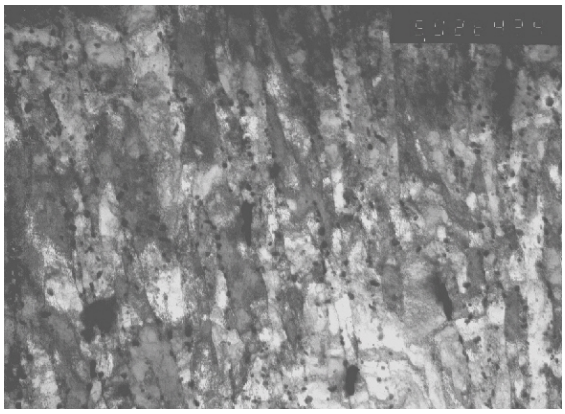

Figure 22 Agglomerates of particles of at interlath boundaries of tempered martensite in sample 580°C/5000h

Figure 23 Dark field image of an inter-lath two-component carbide: $M_{23}C_6$+M_6C in sample 580°C /5000h

M_7C_3. Samples annealed at 500°C also contained evidence of fine carbides within the subgrains. These carbides were identified by selected-area diffraction as mainly cementite and MC phase (V_4C_3). Higher density of the partly spheroidised carbides appeared along the prior austenite grain boundaries; their sizes and density matched those observed on the intercrystalline fracture facets as observed by FEG-SEM.

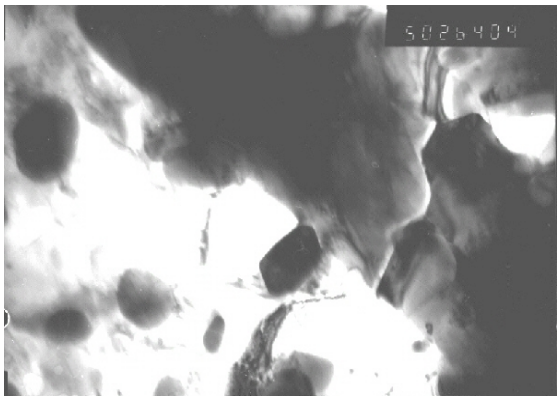

Figure 24 Cracked M_6C carbide in sample 580°C/5000h, deformed to strain 0.07 at 580°C; visible V_4C_3 particle at its side.

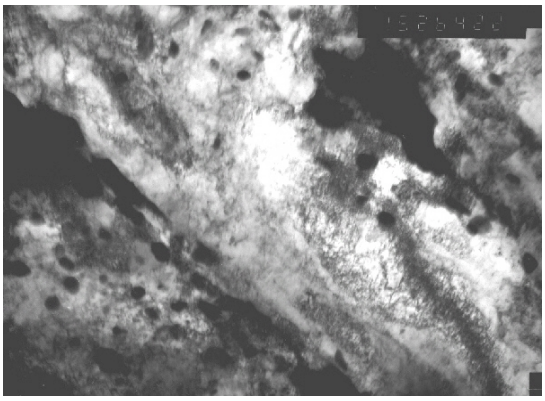

Figure 25 Agglomerates of M_6C carbides on both sides of carbide-free ferrite grain, in sample 580°C/5000h

After annealing at 580°C, the agglomerates of larger particles were seen at the prior austenite grain boundaries, Figure 21, but not only there. Smaller agglomerates were also present at the former martensite interlath boundaries, Figure 22. In the agglomerate's vicinity the ferrite grains were often recrystallised, containing numerous smaller spheroidised carbides. The plate-like carbides, appearing in the agglomerates at interlath boundaries, were identified as $M_{23}C_6$ and M_6C, Figure 23, and even their orientation-relationship could be found (common axis [001]) suggesting their epitaxial growth on one another and at the expense of the other, suggesting quasi in-situ transformation. Selected-area diffraction identification of the large carbides in the agglomerates indicated that they were almost exclusively of the M_6C type.

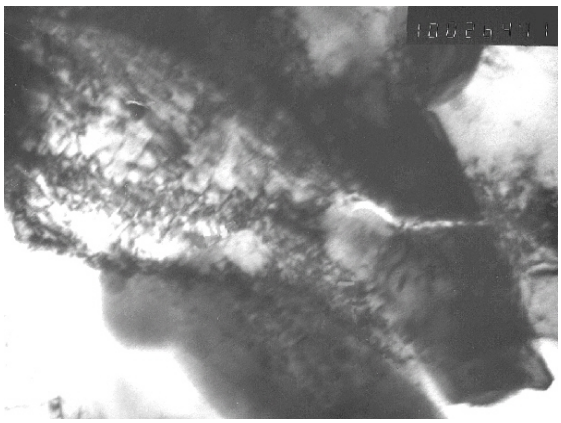

Figure 26 Dislocation pile-up / shear band cutting through M_6C carbide in 580°C/5000h, deformed to strain 0.12 at 540°C(TEM)

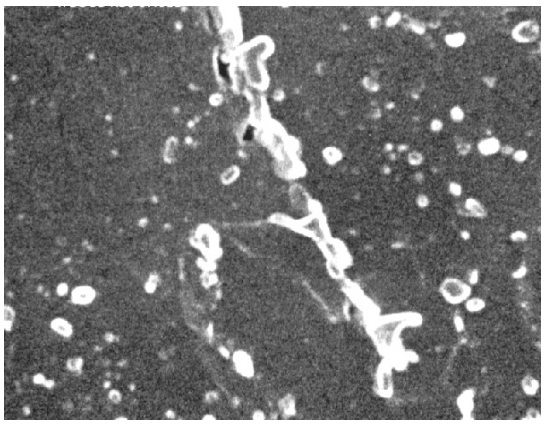

Figure 27 Voids formed at agglomerates of M_6C carbides at PAGB in sample 580°C/5000h, deformed to strain of 0.25 at 580°C(SEM)

Minor amounts of $M_{23}C_6$ and V_4C_3 carbides were also found in these agglomerates. Sometimes the V_4C_3 carbides were attached to, or embedded in the M_6C carbides, Figure 24.

EDS microanalysis of the carbon content, carried out at low voltages in FEG-SEM on thin foils containing the SAD identified M_6C carbides, gave almost stoichiometric results for the M_6C carbides, i.e. between 12 and 14at % C. In examples where $M_{23}C_6$ and V_4C_3 carbides (embedded in the M_6C) were seen in the field of analysis, the measured C content was 15 to 18 at%.

As expected, the plate like carbides in the agglomerates were brittle, and easily separated after the application of small strains. Cracks could be seen between carbide plates on specimens taken from the conical mount portions of the modified SICO samples. An example given in Figure 24, is of 580°C/5000h material deformed to a strain of 0.07 at 580°C. The agglomerates in the 580°C/5000h material often appeared in "parallel arrays" on opposite sides of larger ferrite grains near to the prior austenite grains. This ferrite was often carbide-free, but highly dislocated at small strains below the recrystallisation temperature, Figure 25, which suggests a strain localization mechanism. The dislocations tended to pile-up in the form of shear-bands cutting through the M_6C particles, Figure 26. The examples of Figure 25 and Figure 26 are of the 580°C/5000h material deformed to 0.12 strain at 540°C. The separations between the carbides did not seem to assist any nucleation of the intergranular cracks at elevated temperatures. They did, produce blunting voids near to the carbide agglomerates, Figure 27. Such voids, could have been the reason for the difficulty to produce good quality thin foil specimens from some states of the investigated material.

CONCLUSIONS:

1. The observation of carbides and the sequence of their appearance in the investigated steel is consistent with the IMR-SAS results on precipitation kinetics at temperatures between 500-700°C in Cr-Mo-V low alloy steels.
2. The relatively high Si content in the M_6C carbides may be due to their in-situ transformation from $M_{23}C_6$ carbides, for which the high Si content has been reported elsewhere [4].
3. The M_6C carbides can dissolve substantial amounts of P, thus causing a decrease of the overall P amount of the intercrystalline fracture facets, These fracture facets were not always prior austenite grain boundaries.
4. The appearance of the M_6C carbides in various locations, including prior austenite grain boundaries as well as locations from the boundaries, often causes deviations of the brittle crack path from these boundaries. Thus the fracture surfaces show widespread evidence of substantial local ductile deformations preceding the crack extension.
5. It is hard to imagine that on such rough and complex fracture surfaces a continuous films of contaminants (e.g. P) could be formed and further detailed studies are needed to solve this problem and adequately address the phenomenon of the embrittlement.

ACKNOWLEDGMENTS

STM expresses his gratitude to Hitachi Ltd. / Nissei-Sangyo GmbH, Ratingen, Gemany, for the availability of the S-4700 cold field-emission gun scanning electron microscope with EDS

microanalytical facility. JR acknowledges the use of the MSSI facilities, and Prof. Simon Newcomb for conducting the TEM work at the University of Limerick

REFERENCES

[1] A. Vyrostkova et al. – "Some aspects of phosphorus grain boundary segregation in low alloy steels"; International Workshop of COST 517 Action, Rez, Czech Republic, December 1999 (in print in the Workshop's Proceedings).
[2] R.G.Baker & J.Nutting – Journal of Iron and Steel Institute, 1959, vol.192, p.257.
[3] J.H.Woodhead & A.G.Quarrell – JISI, 1965, vol.203, p.605.
[4] S.T.Mandziej, J.Marciniak – "TEM investigation on in-situ transformation of $M_{23}C_6$ carbides"; Proceedings XIth Congress in Electron Microscopy, Kyoto, Japan, 1986, p.1271.